OPEN ACCESS

University of BRISTOL

Palov, A. P., Balint-Kurti, G. G., Voronina, E. N., & Rakhimova, T. V. (2018). Sputtering of Si by Ar: A binary collision approach based on quantum-mechanical cross sections. *Journal of Vacuum Science and Technology A: Vacuum, Surfaces and Films*, *36*(4), [041303]. https://doi.org/10.1116/1.5027387

Publisher's PDF, also known as Version of record

Link to published version (if available):
10.1116/1.5027387

Link to publication record in Explore Bristol Research
PDF-document

## University of Bristol - Explore Bristol Research
### General rights

# Sputtering of Si by Ar: A binary collision approach based on quantum-mechanical cross sections

Alexander P. Palov, Gabriel G. Balint-Kurti, Ekaterina N. Voronina, and Tatyana V. Rakhimova

## Articles you may be interested in

# Sputtering of Si by Ar: A binary collision approach based on quantum-mechanical cross sections

Alexander P. Palov[a]
*Skobeltsyn Institute of Nuclear Physics, Lomonosov Moscow State University, Moscow 119991, Russia*

Gabriel G. Balint-Kurti
*Centre for Computational Chemistry, School of Chemistry, University of Bristol, Bristol BS8 1TS, United Kingdom*

Ekaterina N. Voronina
*Faculty of Physics and Skobeltsyn Institute of Nuclear Physics, Lomonosov Moscow State University, Moscow 119991, Russia*

Tatyana V. Rakhimova
*Skobeltsyn Institute of Nuclear Physics, Lomonosov Moscow State University, Moscow 119991, Russia*

A new binary collision approach for the calculation of the sputtering yield of Si under nonreactive ionic bombardment by $Ar^+$ is presented for the energy range from threshold to 200 eV. Unlike conventional Monte Carlo approaches that use a classical calculation of the scattering angle from a known potential, their approach employs quantum-mechanical methods to compute the scattering angle. Comparison of the energy and angular dependence of sputtering yields computed using their new quantum-based method with experimental data and with transport of ions in matter (TRIM) and molecular dynamics (MD) calculations supports the accuracy and usefulness of their approach. It is shown that their new approach leads to results of an accuracy intermediate between that of the TRIM and MD methods. The authors expect the new approach to be useful in plasma processing applications. *Published by the AVS.* https://doi.org/10.1116/1.5027387

## I. INTRODUCTION

Argon is often used as an auxiliary gas in plasma processing to provide an anisotropic etch of thin films in a plasma of fluorocarbonates (for instance, $CF_4$ and $CF_3I$),[1,2] to clean film surfaces in oxygen plasma[3] or to perform atomic layer etching in combination with chlorine.[4] These films may consist of pure silicon, its oxide[5] or, for example, of porous organosilicate glasses based on silicon oxide matrices with methyl groups surrounding nanopores.[6]

Incident Ar atoms sputter Si films and break bonds during the interaction. Some empirical formulas for processes such as sputtering yield, reflection probabilities, and for angular and energy distribution functions of ejected atoms from films are often used to model sputtering arising during the etching process.[7] Unfortunately, experimental data are sparse[8–11] and molecular dynamics (MD) calculations[12–16] are used to complement the shortage of required data. However, even for today's computers, the MD method is still time consuming when used to model practical etching situations and faster and more robust procedures are required.

The Monte Carlo (MC) method is a good candidate for this role, but the existing codes such as transport of ions in matter (TRIM) (Refs. 17–19) work best for incident atom energies exceeding a few hundred electron-volt and the predicted angular dependence of the sputtering yield differs significantly from the experimental one.[20] The semiconductor society needs a 3D code to operate at energies in the energy interval of 0–200 eV and to be faster than or comparable with the 1D TRIM.

The goal of this paper is to present a binary collisional approach based on quantum-mechanically computed cross sections (BCA-QM) that is capable of predicting the sputtering yield and its angular dependence in good agreement with experimental or MD results at low energies of incident argon atoms. Unlike conventional MC approaches, based on classical mechanical calculations of the scattering angle, our model uses elastic atom-atom quantum-mechanical differential cross sections (QM-DCS) to compute the scattering angle after a collision. Our approach works in the same manner with both, repulsive and attractive interatomic potentials.

We chose the argon-silicon system because it is the most widely studied both experimentally and computationally by the MC and MD methods, the studies having extended over the last 30 years. The energy and angular dependence of silicon sputtering yields are calculated and compared with data available from the literature.

This paper is organized as follows: in Sec. II, we present empirical and *ab initio* interatomic potentials, the corresponding elastic QM-DCS's and integral cross sections (QM-ICS) and the details of the Monte Carlo algorithm used. In Sec. III, we use the computed QM-DCS's and QM-ICS's to calculate the sputtering yields and their angular dependence for silicon films under low energy argon atom bombardment and, where possible, compare the results obtained with experimental data, TRIM and MD calculations. Finally, Sec. IV gives an overview of our results.

---

[a]Electronic mail: a_palov@mail.ru

## II. PHYSICAL MODEL

### A. General items

From the general view point, the interaction of an ion or atom with the surface of a nano-object should be treated quantum mechanically to describe properly the wave nature of the incident particle, the breaking of bonds in the object, the excitation of different vibrational modes, and so on. In this case, one needs to use the time-dependent n-body Schrödinger equation. Such software packages do exist, for instance, the multi configuration time dependent hartree (MCTDH) code of Mayer *et al.*,[21] but are impractical for the field of sputtering because even for eight particles we already need 18 variables.

The task looks easier if we describe the heavy particle movements classically, but use quantum-mechanical calculations to solve the electronic problem which gives rise to the n-body potential governing the heavy particle or nuclear motion. This may be done for example, by using density functional theory (DFT) as implemented, for instance, in the Vienna Ab initio simulation package code, to generate the forces acting on the nuclei at every time step of a classical dynamics simulation. Such an approach is possible only for systems containing at most a few hundred particles and is used for understanding possible chemical reactions on surfaces.

The task can be simplified if, instead of performing the arduous DFT calculations at each time step of a classical dynamical calculation, we instead use an analytic model potential to determine the forces acting during the classical trajectories. This approach is referred to as the MD method. This method is capable of application to systems of up to a few hundred thousand particles and is widely used in physics applications. The MD n-body potentials are not for reliable atom-atom separations of less than the equilibrium separations and cannot be applied for the modeling of high energy collisions.[22]

At high energies, something above around 1 keV, atomic trajectories can be considered to be straight lines between collisions which can be described by a binary (two-body) potential to determine the scattering angle and the atomic mean free path (MFP) in a solid. This BCA can be used with a system containing up to several million particles.

At present, there are also hybrid methods combining BCA with MD to describe the bombardment of solids with high energy atoms. The BCA method is used for high collision energies and the method switches to using the MD approach at some predefined lower collision energy. The number of atoms that may be treated using the MD method is limited to on the order of a hundred thousand particles.[23] Solving any practical plasma processing task, for instance, sputtering of a 12 nm trench in a solid 200 nm film needs at least around $5 \times 10^6$ atoms in the computing domain, and thus it is difficult to find an alternative to the BCA method for such an application. As a result, this method has been intensively used at ion energies far below 1 keV, which is the limit of where it may be considered to be reliable. It will be shown below that the sputtering yield calculated with BCA gives acceptable results for normal incidence even for

energies from the threshold to 200 eV. However, its angular dependence is very far from the MD results. The basic question is: is there a way to improve the BCA method so as to obtain angular dependencies closer to MD results? To address this question, we outline the traditional BCA method using classical mechanics. We will denote this approach as the BCA-C method.

First, the impact parameter $R_o$ (the distance of closest approach of two collision partners in the absence of any potential, see Ref. [33]) is obtained using a random number generator, after that the angle of scattering in the center-of-mass reference frame is calculated from classic formulas for a known interatomic potential. Following this the angle of scattering relative to the direction of the traveling particle is calculated, and the direction of particle movement in the laboratory system is obtained. Energy loss after a collision is calculated and a mean free path is determined, a total scattering cross section which is estimated using the average interatomic distance in a solid. Note, normally in the BCA-C method, scattering by angles less than $0.5°$–$1°$ are neglected because this would require a great increase in the impact parameters used in the calculation. In addition, Eckstein[24] has shown that the classical approach for the small angle scattering is insufficiently accurate.

In contrast to classical mechanics, quantum mechanics has no difficulty in computing small angle scattering. For a realistic atom-atom potential, which has no arbitrary cut-off at large separations, classical mechanics predicts an infinite total cross section, while quantum mechanics gives rise to a finite cross section. Therefore, in order to overcome these problems, which arise when using classical mechanics, we propose to use quantum mechanics (QM) to compute the angle dependent differential cross sections and the total or integral cross sections. We denote this binary collision approach quantum mechanical method as BCA-QM. The first two introductory chapters of our book "Theory of Molecular Collisions"[33] contain definitions of the standard quantities such as "impact parameter" and "differential cross section" used in this paper.

### B. Interatomic potentials

The most frequently used Ar-Si interatomic potential in conventional MC models is the empirical one of Moliere.[25] In order to test the dependence of our BCA-QM model on different interatomic potentials of the Ar-Si pair we considered that of Moliere and an analytic fit to the DFT potential by Hossain *et al.*[26] In addition to this comparison, we have also added a more accurate *ab initio* binary potential that we have calculated ourselves. The analytic form of these three potentials can be presented in the Ziegler-Biersack-Littmark (ZBL) type

$$V_{ij}(r) = \frac{Z_i Z_j}{r} \sum_{k=1}^{n} \alpha_k \exp\left(-\beta_k \frac{r}{a}\right), \tag{1}$$

where $r$ and $a = 0.4683(Z^{\gamma 1} + Z^{\gamma 2})^{-\gamma 3}$ are given in Å, the potential $V_{ij}(r)$ is given in eV, and dimensionless coefficients $\alpha$, $\beta$, and $\gamma$ are given in Table I.

Our atom-atom or pure binary potential was calculated with help of MOLPRO package (version 2012.1)[27,28] for the ground electronic state of the ArSi($^3\Sigma^-$) molecule. To achieve high accuracy, we used the largest available atomic orbital basis (AV6Z) and a restricted Hartree–Fock calculation followed by a complete active space (CAS) self-consistent field method computation at each interatomic separation. These results are labeled as CAS in Table I and in the rest of the paper.

The most popular and simple three-body interatomic potential for Si in MD calculations is the one of the Stillinger-Weber's (SW)[29] type. We decided to use its binary part considering the attraction between Si atoms with coefficients obtained from Hartree-Fock calculations[30] (see Table II)

$$V_{ij}(r) = \begin{cases} A_{ij}\left(B_{ij}r_{ij}^{-p_{ij}} - r_{ij}^{-q_{ij}}\right)\exp\left[(r_{ij} - a_{ij})^{-1}\right], & r_{ij} < a_{ij} \\ 0, & r_{ij} \geq a_{ij}, \end{cases}$$
(2)

where $a_{ij}$ is a cut-off radius. The potential $V_{ij}(r)$ is given in Hartree, the radii $r_{ij}$ is the interatomic distance between $i$-th and $j$-th atoms. Both the $r_{ij}$ and the $a_{ij}$ radii are given in Angstrom divided by 2.0951 Å, so they are dimensionless. The symbols "$i, j$" indicate index numbers of the particular Si atoms being considered.

Figure 1 shows three Ar-Si and one Si-Si interatomic potentials used in our MC modeling of sputtering of Si films bombarded by low-energy Ar neutral atoms. The Si-Si potential can be seen to possess an attractive part while all Ar-Si potentials are purely repulsive.

## C. Differential and integral cross sections

In classical mechanics the polar angle of scattering in center-of-mass coordinates can be calculated using the formula[31–33]

$$\theta(E, b) = \pi - 2b \int_{r_o}^{\infty} \frac{dr}{r^2\sqrt{1 - \dfrac{b^2}{r^2} - V(r)/E}},$$
(3)

where $\theta(E, b)$ is the deflection angle, $E$ is the relative kinetic energy, $V(r)$ is the potential, and $b$ is the impact parameter.

Figure 2 presents such deflection angles calculated for $E = 10$ eV for both a repulsive ArSi CAS and the partly attractive SiSi SW potentials. In the case of ArSi, the deflection angle remains within the range of 0°–180°. For the SiSi pair, the potential possesses an attractive part and the deflection angle takes on negative values as well. The presence of negative values of the deflection angle necessitates using the

TABLE I. Parameters for the interatomic potentials of ZBL type for Ar-Si atomic pair [see Eq. (1)].

|         | $\alpha_1$ | $\alpha_2$ | $\alpha_3$ | $\beta_1$ | $\beta_2$ | $\beta_3$ | $\gamma 1$ | $\gamma 2$ | $\gamma 3$ |
|---------|-----------|-----------|-----------|-----------|-----------|-----------|-----------|-----------|-----------|
| Moliere | 0.35      | 0.55      | 0.1       | 0.3       | 1.2       | 6.0       | 0.5       | 0.5       | 0.667     |
| DFT     | 0.196     | 1.368     | 4.513     | 0.257     | 2.322     | 2.446     | 0.22      | 0.22      | 1.0       |
| CAS     | 3.932     | −2.38     | 10.037    | 5.566     | 4.805     | 26.68     | 0.22      | 0.22      | 1.0       |

TABLE II. Parameters for the interatomic potential of SW type for Si-Si atomic pair (Ref. 26) [see Eq. (2)].

| Si-Si | |
|-------|-------------|
| $A_{SiSi}$ | 7.049556277 |
| $B_{SiSi}$ | 0.6022245584 |
| $p_{SiSi}$ | 4 |
| $q_{SiSi}$ | 0 |
| $a_{SiSi}$ | 1.8 |

slow Gauss-Mehler integration procedure instead of the faster "Magic" one[17] in conventional Monte Carlo programs.[34,35]

The classic DCS (C-DCS) must be calculated as[27]

$$\frac{d\sigma}{d\Omega} = \sum_i \frac{b_i}{\left|\sin\theta\left(\dfrac{d\theta}{db}\right)_i\right|},$$
(4)

where the summation is taken over all values of $b$ which contribute to scattering into the angle $\pm\theta$.

Figures 3(a) and 3(b) show computed C-DCS's for ArSi CAS and SiSi SW potentials as smooth lines. A basic problem of the classical approach is that the C-DCS always diverges for forward scattering because $\sin\theta$ tends to zero as $\theta$ decreases to zero. If the potential has an attractive portion the C-DCS diverges also at the point of the minimum of the deflection angle around $\theta_y = 50°$ in the present case for Si-Si. This happens because $d\theta/db = 0$ in the denominator of Eq. (4). The computed QM-DCS's are shown as oscillating lines in Fig. 3. The computed QM-DCS's do not possess any singularities. Owing to the singularities present in the computed C-DCS's, they cannot be used for scattering at around 0° or for potentials with an attractive part.

If the C-DCS is used, increasing the impact parameter $b$ will lead to unconstrained growth of the C-DCS in the
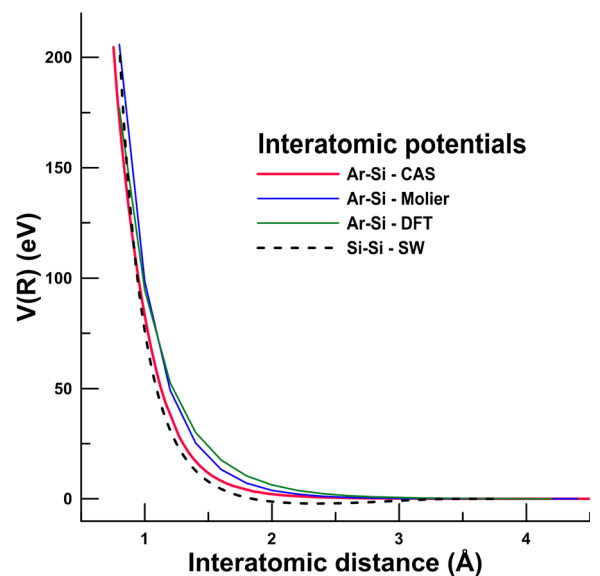


FIG. 1. (Color online) Interatomic potentials as a function of the interatomic distance.
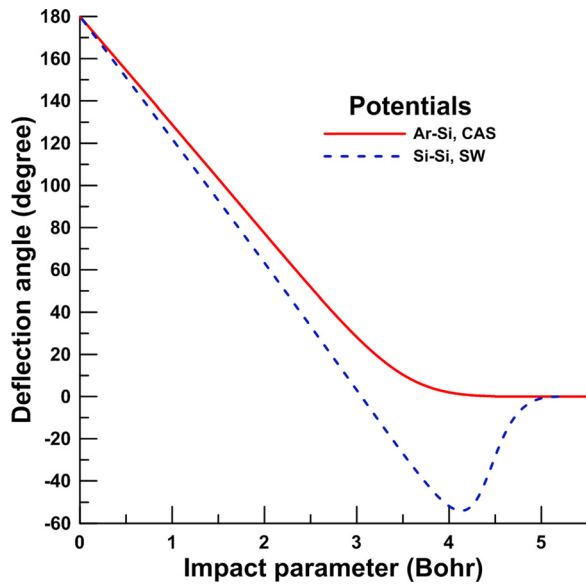
FIG. 2. (Color online) Deflection angle for ArSi (calculated using the CAS potential and shown by solid line) and SiSi (calculated using the SW potential and shown by dashed line) potentials calculated at the relative kinetic energy of 10 eV. The deflection angle is a quantity defined in the classical mechanics of atom-atom scattering. See Chap. 1 of Ref. 33.

vicinity of $\theta = 0°$ and as a consequence to an overestimation of the scattering probability in the range of small angles.

The classical ICS (C-ICS) for a potential of finite range converges because for impact parameters greater than the range of the potential there will be no scattering or deflection. In such cases, the C-ICS will be given by $\pi\rho^2$, where $\rho$ is the range of the potential. This range parameter is normally quite arbitrary, and the C-ICS will be entirely dependent on its choice. Because of these problems, the majority of Monte Carlo approaches are based on the mean free path taken as the average interatomic distance in a solid or as a semiempirical parameter.[36] In contrast, the computed QM-ICS is finite even for potentials of infinite range, such as Lennard–Jones or ZBL potentials.

Our idea is to apply quantum mechanics to calculate the DCS's because they do not diverge for any real interatomic potential. An additional advantage is that we obtain the QM-ICS and need not use any semiempirical parameters to define them. Below we outline briefly some formulas needed to compute the QM-DCS and QM-ICS for atom-atom collisions, for the computation of the relevant scattering angles after collisions and for the calculation of the MFP of an atom in a solid.

The basic quantity required for the calculation of a QM-DCS or QM-ICS is the scattering phase shift.[29,37] We applied the Jeffreys-Wentzel-Kramers-Brillouin (JWKB) approximation to compute the scattering phase shift, $\delta_l(E)$. These phase shifts were calculated using the Langer correction[38] to the centrifugal part of the effective potential

$$\delta_l^{\mathrm{JWKB}}(E) = \int_{r_2}^{r_{\max}} \left\{ 2\mu_{\mathrm{AB}}E - 2\mu_{\mathrm{AB}}V(r) - \frac{(l+1/2)^2}{r^2} \right\}^{1/2} dr$$
$$- \int_{r_1}^{r_{\max}} \left\{ 2\mu_{\mathrm{AB}}E - \frac{(l+1/2)^2}{r^2} \right\}^{1/2} dr, \qquad (5)$$

where $\mu_{\mathrm{AB}}$ is the reduced mass of molecule consisting of atoms A and B, $r_{\max}$ is the maximal interatomic separation [beyond which $V(r)$ is taken to be zero], $r_1$ and $r_2$ are the classical turning points for the centrifugal and effective potentials, respectively.

When the scattering phase shifts are known, the QM-DCS in the center-of-mass reference frame for nonidentical particles such as Ar-Si is given by

$$\frac{d\sigma_{\mathrm{CM}}}{d\Omega}(E,\theta) = \frac{1}{k^2} \left| \sum_{l=0}^{\infty} (2l+1) e^{i\delta_l(E)} \sin\delta_l P_l(\cos\theta) \right|^2, \quad (6)$$

where $d\Omega = \sin\theta d\theta d\phi$ is the solid angle, $P_l(\cos\theta)$ is the $l$-th Legendre polynomial, $\theta$ is the center-of-mass scattering angle, $\varphi$ is the azimuthal angle, and $k = \{2\mu_{\mathrm{AB}}E/\hbar^2\}^{1/2}$ is the wave vector of the relative motion. For identical
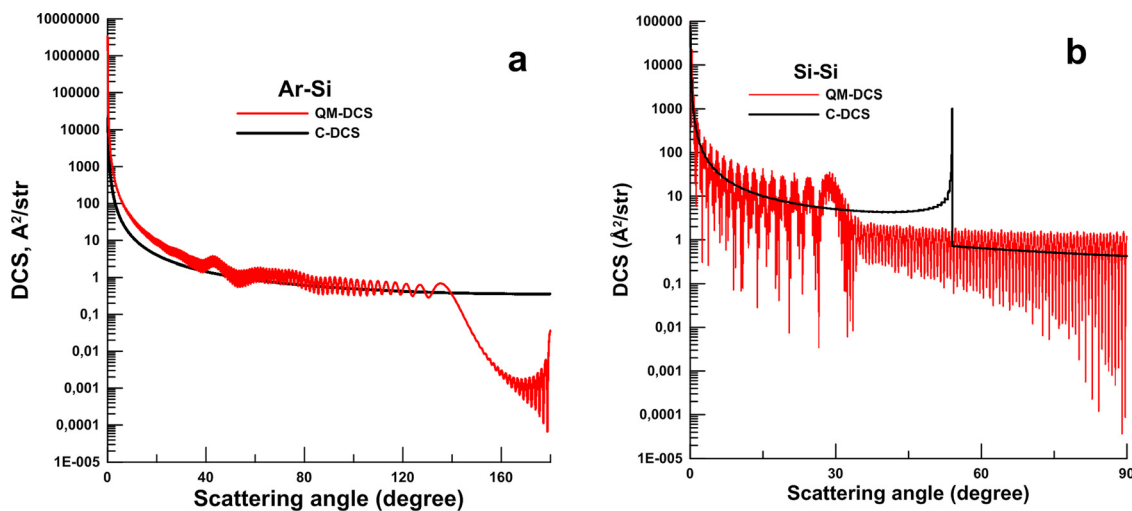


FIG. 3. (Color online) C-DCS and QM-DCS for Ar-Si (a) and Si-Si (b) pairs in the center-of-mass reference frame calculated at relative kinetic energy of 10 eV. For Ar-Si the CAS and for Si-Si the SW potentials were used. See Chaps. 1 and 2 of Ref. 33 for discussion of classical and quantum mechanical cross sections (C-DCS and QM-DCS).

particles, in our case, it is a Si-Si pair, and the QM-DCS is given by

$$\frac{d\sigma_{CM}}{d\Omega}(E,\theta) = \frac{2}{k^2}\left|\sum_{l=0,2,4..}^{\infty}(2l+1)e^{i\delta_l(E)}\sin\delta_l(E)P_l(\cos\theta)\right|^2.$$

(7)

The QM-DCS for Ar-Si and Si-Si atomic pairs are presented as red lines in Figs. 3(a) and 3(b), respectively. The main properties of the two QM-DCS's are that they do not diverge anywhere, have sharp, but finite, maximums at zero angles. The Ar-Si QM-DCS decreases sharply as the angle increases, possessing almost negligible values at large angles. In the case of the identical atoms, in our case, the Si-Si pair [see Fig. 3(b)], the QM-DCS, is symmetric about $\theta = 90°$. In this case, the QM-DCS becomes negligible in the vicinity of 90°. The QM-ICS is obtained by integrating Eqs. (6) and (7) over all polar and azimuthal angles. Thus, we get for nonidentical and identical particles, respectively,[29,33]

$$\sigma_{AB}(E) = \frac{4\pi}{k^2}\sum_{l=0}^{\infty}(2l+1)\sin^2\delta_l(E),$$

(8)

$$\sigma_{AA}(E) = \frac{8\pi}{k^2}\sum_{l=0,2,4..}^{\infty}(2l+1)\sin^2\delta_l(E).$$

(9)

Figure 4 shows the QM-ICS's for atomic pairs involved in sputtering Si films by Ar atom. The Ar-Si potentials are all purely repulsive, and consequently, the QM-ICS's all decrease quite smoothly with increasing collision energy. This is particularly true at higher collision energies. As mentioned earlier, Si-Si has an attractive part. As a result, the QM-ICS displays some pronounced oscillations, known as Glory oscillations. The QM-ICS arising from the use of the DFT potential of Hossain[22] is 25% greater than Moliere's ones, while our CAS potential yields an QM-ICS of some
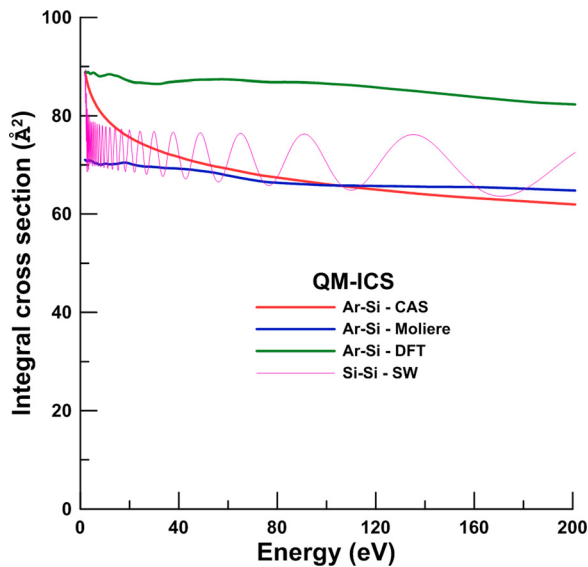


FIG. 4. (Color online) Dependence of the QM-ICS on the relative kinetic energy for Si-Si and Ar-Si atomic pairs.

average magnitude to the two others. The ICS is obtained by integrating the DCS over all angles. For a realistic interaction potential, which continues out to infinite separation and has no artificial cut-off, the C-DCS becomes infinite at small scattering angles [see Fig. 3(a)]. This results in an infinite C-ICS which cannot therefore be used. In the case of the SW potential [used for Si-Si in Fig. 3(b)], the potential has an artificial cut-off at some large internuclear separations. This arbitrary cut-off radius determines the magnitude of the C-ICS in this case. Note that the QM-ICS for a hard sphere model is independent of collision energy and is twice as large as that of the C-ICS for the same hard sphere model.[33]

During Monte Carlo modeling, the polar angle $\theta_X$ after every collision was calculated from the transcendent equation

$$\xi\sigma_{AB}(E) = 2\pi\int_0^{\theta_X}\frac{d\sigma_{CM}(E)}{d\Omega}\sin\theta d\theta,$$

(10)

where $\xi$ is a random number between 0 and 1.

The azimuthal angle was uniformly distributed in the range of 0–2π. The right hand side of Eq. (10) is computed for a range of the two parameters E and $\theta_X$, tabulated, and used in a MC program to extract the polar angle for a given random number. In comparison to the conventional classic impact parameter approach, there is no need to compute a deflection angle, or in other words, there is no need to compute the collision integral, and this greatly accelerates the modeling.

The MFP of the A atom in a solid with concentration of B atoms $n_B$ was defined using the following "gaseous" formula:

$$\ell_{AB}^{-1}(E) = n_B\sigma_{AB}(E).$$

(11)

In case of a solid consisting of a few different kinds of atoms the inverse MFP should be calculated as

$$\ell_A^{-1}(E) = \ell_{AB}^{-1} + \ell_{AC}^{-1} + ....$$

(12)

Finally, during Monte Carlo modeling, the MFP was extracted from

$$\ell(E) = -\ell_A(E)\ln\xi.$$

(13)

### D. Monte Carlo algorithm

The MC algorithm used can be described as the follows: the MFP of an incident atom in a film is calculated from Eq. (13). Then, a recoil atom is chosen for a collision, and the scattering angle in the center-of-mass reference frame is taken for this atomic pair from the table obtained with Eq. (10). The energy transfer and directions of movement for both atoms after the collision are calculated from the energy and momentum conservation laws.

Some elements of solids are nevertheless used in our gaseous model such as the surface binding energy $E_{SBE}$ and the lattice binding energy $E_{LBE}$. It has been suggested that they

are related by equation $E_{LBE} = 2E_{SBE}$, and for the near-surface layer, the following model formula is used:[39]

$$E_{extr} = \begin{cases} E_{SBE}, & z = 0 \\ E_{SBE} + (E_{LBE} - E_{SBE})\dfrac{z}{d}, & 0 < z < d \quad (14) \\ E_{LBE}, & z \geq d, \end{cases}$$

where $E_{extr}$ is the energy needed to extract an atom from a solid, $z$ is the atomic position relatively to the surface of the solid, and $d \sim 1\,nm$ is twice the value of the lattice constant. If the energy transferred to a recoiling atom is higher than $E_{extr}$, a secondary atom is generated. If the energy of the primary atom is then less than $E_{extr}$, we treat it as being trapped.

In practice, one needs a 3D code which is able to describe sputtering of materials with arbitrary shape and porosity. To make this possible, we have implemented the physical model mentioned earlier within a MC algorithm based on Cartesian coordinates in 3D with a cubic cell size of $0.272 \times 0.272 \times 0.272\,nm^3$ and applied it in this paper just to a flat solid film. Our 3D map generator was applied to generate such a grid.[6] The area of calculation included a film with a depth of $z = 180\,nm$ and surface $S = x \times y$ of $x = 24\,nm$ and $y = 24\,nm$ with periodic boundary conditions in x and y directions. At present, the code has an upper energy limit of 200 eV because of the need to use large arrays arising from the implementation of Eq. (10).

Figure 5 presents an example of sputtering of 12 nm trenches in solid and porous silicon films under 200 eV argon bombardment with dose of $2.1 \times 10^{17}\,cm^{-2}$ calculated by our 3D MC code. The pore size radius of 2.4 nm and interconnectivity radius of 2.1 nm were implemented in porous silicon film with the porosity of 40% typical for modern films.
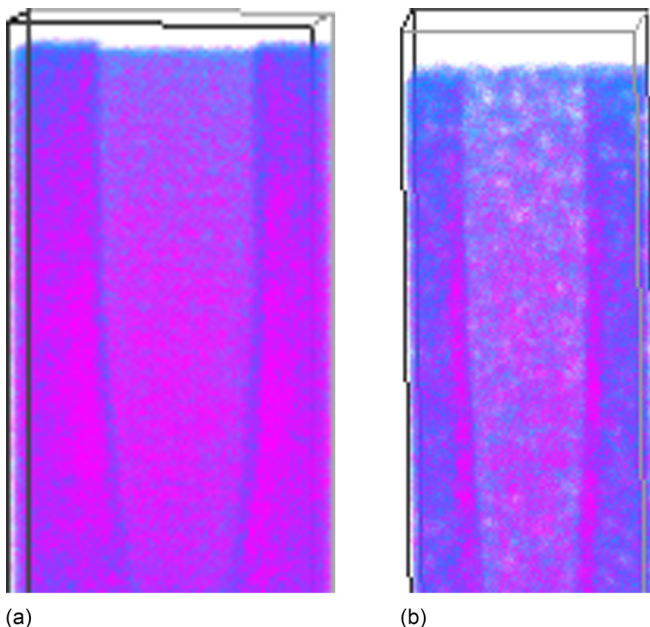
## III. RESULTS AND DISCUSSION

There are only a few published experimental[8–12,36,37] or MD (Ref. 13) investigations of the sputtering of silicon under argon ion bombardment in the range of low energies (20–200 eV). Only two of them[36,37] quote the fluencies of argon ions of $10^{16}$ and $10^{18}\,cm^{-1}$. We have chosen a fluence of $5.21 \times 10^{16}\,cm^{-1}$ that means $3 \times 10^5$ argon trajectories impinging on the surface of $576\,nm^2$.

Figure 6 shows the calculated dependence of silicon sputtering yield on the energy of Ar ions incident normally onto a silicon film surface for three different Ar-Si potentials. The calculated sputtering yields are all very similar. At lower energies, the sputtering yields are almost identical, while at an incident energy of 200 eV, the calculated sputtering yields are still within 10% of each other. The main conclusion from the results of Figs. 4 and 6 is that the difference in the QM-ICS's of around 25% found for the Moliere and DFT-Hassein potentials does not lead to a noticeable change in the calculated sputtering yield.

Figure 7 shows a comparison of the calculated energy dependence of the sputtering yield from amorphous silicon after argon irradiation pointed normally to the surface with experimental data, TRIM and MD calculations. The TRIM calculations were also performed by us using standard parameters. As may be seen, the calculated value of the silicon sputtering yield based on our BCA-QM method (shown in green by dotted-dashed line) is in a reasonable agreement with the latest experimental data (dotted blue line), the TRIM curve given in red and the MD calculations (open circles) are also close to our new results and to the latest experimental results. The older experimental data show large divergences from each other. Probably, more precise experiments are required to obtain a large set of self-consistent data from different authors in the range of low energies of incident argon atoms. The BCA methods are generally



FIG. 5. (Color online) 3D images of 12 nm trenches sputtered by 200 eV argon ions in silicon films with porosities of 0% (a) and 40% (b) with a dose of $2.1 \times 10^{17}\,cm^{-2}$. The calculations were performed using our 3D-MC code together with the BCA-QM method.
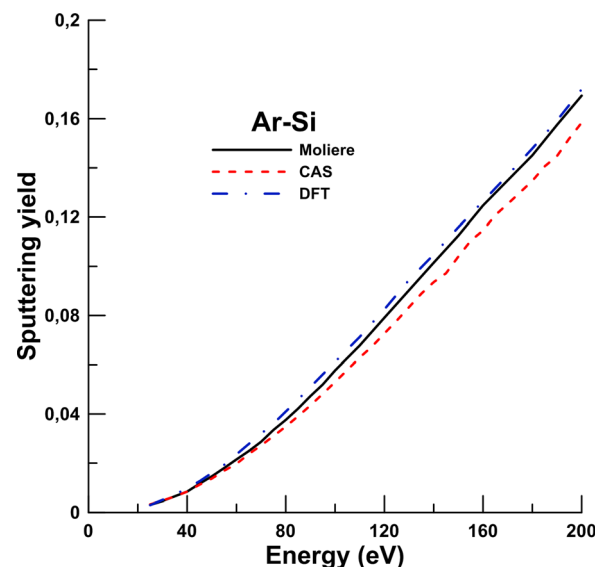


FIG. 6. (Color online) Dependence of silicon sputtering yield on the energy of argon ions incident normally onto a silicon surface, calculated using three different Ar-Si potentials with BCA-QM.
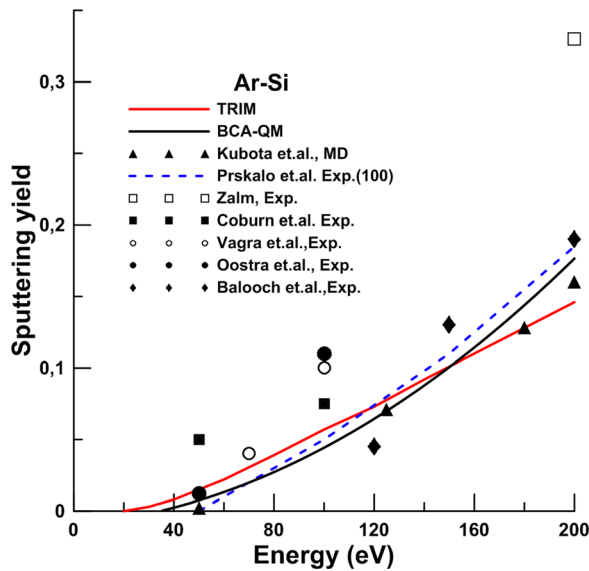
FIG. 7. (Color online) Dependence of silicon sputtering yield on the energy of Ar atoms for the case of normal incidence to the Si surface. Experimental data □ (Ref. 8), ◆ (Ref. 9), ● (Ref. 11), dashed blue line (Ref. 12), ⊠ (Ref. 40), ○ (Ref. 41), and MD calculations ▲ (Ref. 13).

expected to be less reliable at energies below 1 keV where it is thought that MD methods must be used. Our results however demonstrate a good agreement between the BCA-QM method and the MD calculations all the way down to below 100 eV. Note, the difference between all calculated curves does not exceed 20%.

The sputtering yield calculated using our BCA-QM is shown (solid line) in Fig. 8 as a function of the angle of incidence relative to the normal. It was only possible to compare our results with MD and TRIM calculations because of the lack of experimental data. For argon energies below 200 eV, we found just one such MD result obtained at 100 eV.
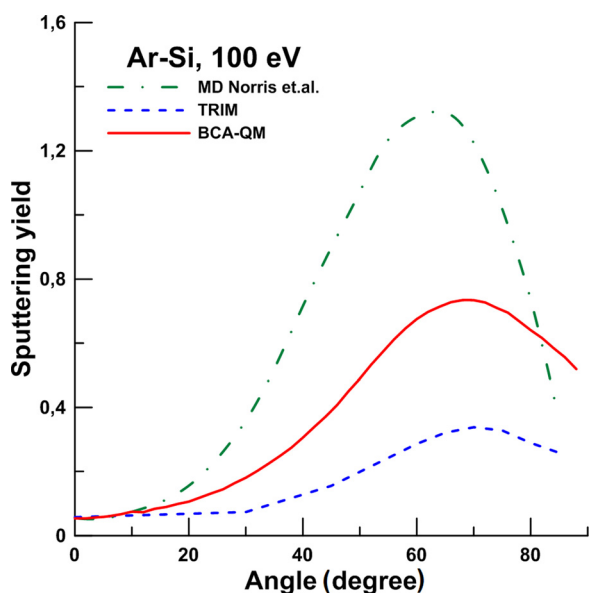
As may be seen from the figure, the MD curve, shown by the dotted-dashed line, predicts the highest yield and has a maximum at 65° while the results of the TRIM calculations give the lowest sputtering yield, represented by the dashed curve, with a maximum located at 74°. Our BCA-QM curve shown as a solid line is placed between these two curves and has a maximum at 69°. Both binary theories show the same behavior at large angles, i.e., they decline gradually in contrary to the curve of the MD method which decreases very steeply with increasing angle. The MD method considers three body interactions and is the most accurate method at present. Our binary model leads to results closer to the MD results than the TRIM method, and thus, we can conclude the BCA-QM is of intermediate accuracy between MD and classic MC calculations based on the conventional impact parameter method.

Using the BCA-QM, we have calculated the angular dependence of the sputtering yield for a set of energies from 50 to 200 eV which are of importance for plasma processing applications. Also, we have also performed this calculation using the TRIM code for energies 50 and 200 eV. The results of these calculations are presented in Fig. 9.

From the figure, one can see that the sputtering yield calculated with the BCA-QM at an argon energy of 200 eV has a maximum at 65°.[35] The same maximal location was obtained using the MD calculations at 100 eV (see Fig. 8) and 250 eV. At lower energies, the calculated maxima of our curves move toward the maximum calculated by TRIM at 50 eV. The absolute values of sputtering yield calculated by our BCA-QM and by the TRIM method are closer at 200 eV and become more different at 50 eV. This can be explained by the known fact that the TRIM method works better for high energies.

The angular distributions of ejected Si and Ar atoms from the silicon surface calculated at $\theta = 30°$ and $\theta = 80°$ incident



FIG. 8. (Color online) Dependence of the silicon sputtering yield on the angle of incidence to the surface normal at an argon energy of 100 eV in comparison to MD (Ref. 42) and TRIM calculations.
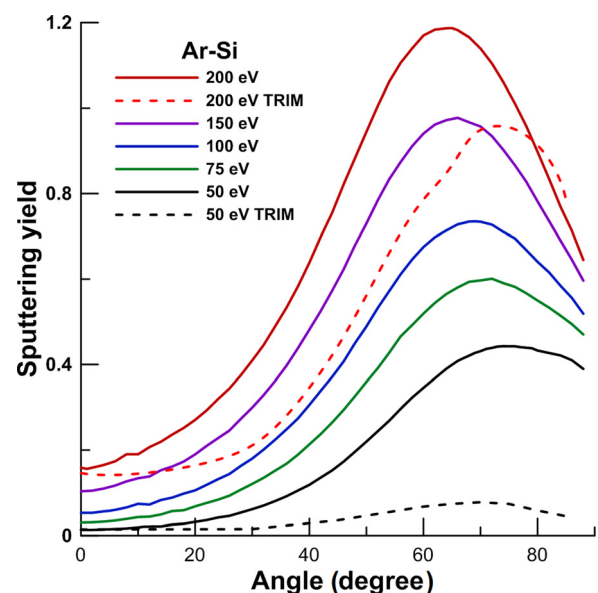


FIG. 9. (Color online) Dependence of silicon sputtering yield on the angle of incidence with the normal to the surface of argon ions at energies from 50 to 200 eV.

angles and at argon ion incident energies of 50 and 200 eV are shown in Figs. 10(a) and 10(b), respectively. Comparison of the figures shows that the positions of the Si angular distribution peak, located at around 55°, is almost independent of the incident ion energy. The positions of the peaks of the angular distribution of ejected Ar atoms move toward higher angles (i.e., from 55° toward 80°) with the increase in the angle of incidence of Ar ions. This can be explained by the fact that at low energy and at grazing angles, the Ar atoms do not penetrate deeply into the silicon lattice and are preferentially reflected. The diffuse character of the distribution may be caused by the roughness of the surface and multiple scattering nature of the Ar atom scattering. A similar behavior of the sputtering yield and reflection probability is found for 200 eV argon ions. The only difference is that the silicon angular distribution peaks are shifted by around 5° toward smaller angles. Thus, for the modeling of Ar atoms reflection from a silicon surface at glazing angles of incidence, one can use the approximate rule that the incident and reflection angles are equal even for low energy particles.

The energy distributions of ejected Si and Ar atoms calculated for incident angles of $\theta = 30°$ and $\theta = 80°$ to the normal for Ar ion energies of 50 and 200 eV are shown in Figs. 11(a) and 11(b), respectively. The energy distributions of the Si sputtered atoms always have peaks at low energies of around 5–10 eV because of the existence of a potential plane barrier at the surface. The main effect of increasing the incident energy from 50 to 200 eV is just to increase the magnitude of the silicon energy distribution function. Increasing the Ar ion incident energy from 50 to 200 eV leads to the growth of the sputtering yield. In contrast to the Si atom distribution, the energy distribution of the reflected Ar atoms depends sensitively on the incident angle. For an incident angle of 80°, an additional energy peak appears close to the initial energy of the argon ions because, in comparison to scattering at an incident angle of 30°, the argon

ions have fewer collisions with silicon atoms at grazing angles before leaving the solid.

## IV. SUMMARY AND CONCLUSIONS

In this paper, we suggest that quantum-mechanical DCS for atom-atom collision should be used to describe atom-atom scattering. This permits a more accurate description of small and large angular scattering in comparison with the classical-mechanical calculations and the computation of the MFP without using semiempirical parameters.

The calculated quantum-mechanical cross sections are tested within an MC framework through the modeling of the sputtering of silicon films under bombardment by low-energy argon ions. The energy and angular dependencies of the sputtering yield obtained agree reasonably with the latest experimental data, and also with TRIM and MD calculations. The angular dependence of the sputtering yield for low-energy argon ions are presented for the first time for a range of incident energies. These quantities have previously only been available for a single energy, namely, 100 eV. Comparison of our angular dependence with TRIM and MD calculations leads to the conclusion that our new BCA-QM method leads to results of accuracy intermediate between these two methods. The BCA-QM is clearly less reliable than the MD method because it does not consider n-body interactions, which are really important for low energy sputtering calculations. The advantage of the BCA-QM method being that it is computationally far faster. Comparison of our BCA-QM results shown in Figs. 7 and 8, as compared with the TRIM and MD results, shows that the improved treatment of the angular scattering seems to make our calculations more reliable at low collision energies and leads to an improved agreement with the superior MD calculations.

The physical model we have developed has been implemented in 3D and is capable of describing sputtering from nanostructures with arbitrary geometry. Our 3D code has the same speed performance as the 1D TRIM method, and we
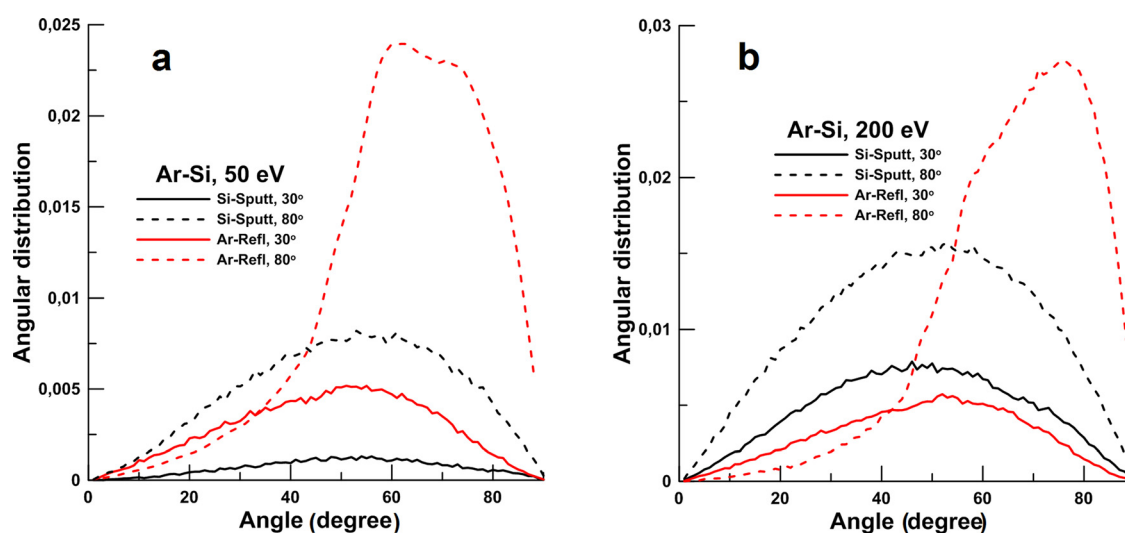


FIG. 10. (Color online) Angular distribution of ejected Si and Ar atoms from the Si surface for two Ar ion energies 50 eV (a) and 200 eV (b) and the angle of incidence to the normal to the Si surface equal to 30° and 80°, calculated with BCA-QM.
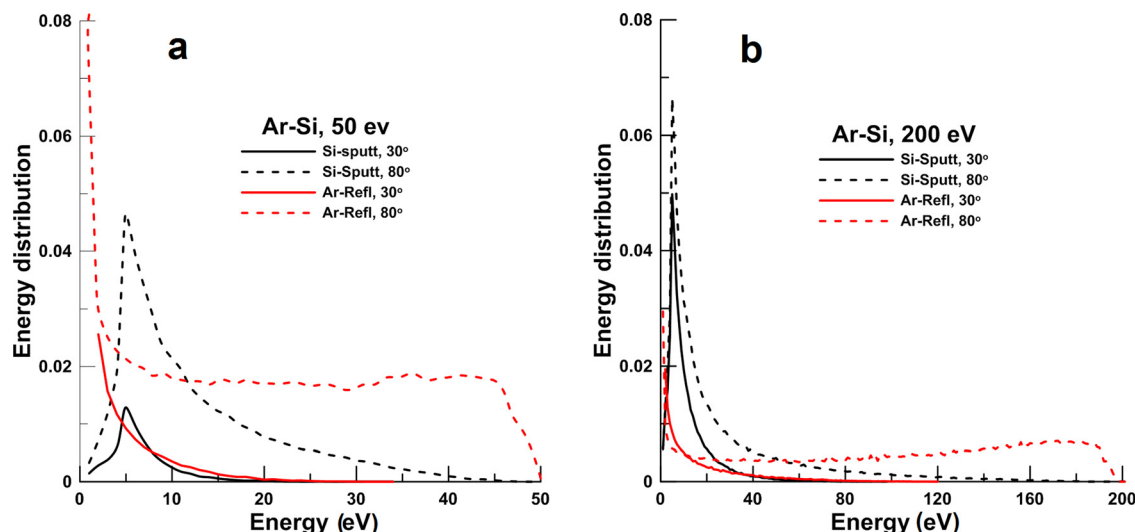
FIG. 11. (Color online) Energy distribution of ejected Si and Ar atoms from the Si surface for two Ar ion energies, 50 eV (a) and 200 eV (b), and an angle of incidence to the surface normal equal to 30° and to 80°, calculated with BCA-QM.

expect it to be capable of efficiently solving real 3D problems in plasma processing.

[1] M. R. Baklanov, J.-F. Marneffe, D. Shamiryan, A. M. Urbanowicz, H. Shi, T. V. Rakhimova, H. Huang, and P. S. Ho, J. Appl. Phys. **113**, 041101 (2013).
[2] A. Agarwal and M. J. Kushner, J. Vac. Sci. Technol., A **27**, 37 (2009).
[3] M.-H. Jung and H.-S. Choi, Thin Solid Films **515**, 2295 (2006).
[4] P. Ventzek, S. D. Sherpa, M. Wang, V. Rastogi, and A. Ranjan, ECS Trans. **75**, 25 (2016).
[5] H. Matsumura, Jpn. J. Appl. Phys., Part 1 **37**, 3175 (1998).
[6] A. P. Palov, T. V. Rakhimova, M. B. Krishtab, and M. R. Baklanov, J. Vac. Sci. Technol., B **33**, 020603 (2015).
[7] A. Sankaran and M. J. Kushner, J. Vac. Sci. Technol., A **22**, 1242 (2004).
[8] P. C. Zalm, J. Appl. Phys. **54**, 2660 (1983).
[9] M. Balooch, M. Moalem, W.-E. Wang, and A. V. Hamza, J. Vac. Sci. Technol., A **14**, 229 (1996).
[10] R. Smith, D. E. Harrison, and B. J. Garrison, Phys. Rev. B **40**, 93 (1989).
[11] D. J. Oostra, A. Haring, R. P. van Ingen, and A. E. de Vries, J. Appl. Phys. **64**, 315 (1988).
[12] A.-P. Prskalo, S. Schmaudera, C. Ziebert, J. Yeb, and S. Ulrich, Comput. Mater. Sci. **50**, 1320 (2011).
[13] N. A. Kubota and D. J. Economou, J. Appl. Phys. **83**, 4055 (1998).
[14] C. F. Abrams and D. B. Graves, J. Vac. Sci. Technol., A **16**, 3006 (1998).
[15] D. Graves and P. Brault, J. Phys. D: Appl. Phys. **42**, 194011 (2009).
[16] D.-H. Kim, G.-H. Lee, S. Y. Lee, and D. H. Kim, J. Cryst. Growth **286**, 71 (2006).
[17] J. P. Biersack and L. G. Haggmark, Nucl. Instrum. Methods **174**, 257 (1980).
[18] J. F. Ziegler, J. E. Biersack, and U. Littmark, *The Stopping and Range of Ions in Matter* (Pergamon, New York, 1985), p. 321.
[19] W. Eckstein, Nucl. Instrum. Methods B **33**, 489 (1988).
[20] H. Hofsäss and K. Zhang, Appl. Surf. Sci. **310**, 134 (2014).
[21] *Multidimensional Quantum Dynamics: MCTDH Theory and Application*, edited by H. D. Mayer, F. Gatti, and G. A. Worth (Wiley-VCH, Weinheim, 2009), p. 381.
[22] A. V. Krasheninnikov and K. Nordlund, J. Appl. Phys. **107**, 071301 (2010).
[23] S. Saito, A. M. Ito, A. Takayama, T. Kenmotsu, and H. Nakamura, J. Nucl. Mater. **415**, S208 (2011).
[24] W. Eckstein, *Computer Simulation of Ion-Solid Interaction* (Springer-Verlag, Berlin, 1991), p. 296.
[25] G. Molière, Z. Naturforsch. **2a**, 133 (1947).
[26] M. Z. Hossain, J. B. Freund, and H. T. Johnson, Nucl. Instrum. Methods, B **267**, 1061 (2009).
[27] H.-J. Werner *et al*., *MOLPRO Version 2012.1 a Package of Ab Initio Programs* (University College Cardiff Consultants Limited, Cardiff, 2012).
[28] H.-J. Werner, P. J. Knowles, G. Knizia, F. R. Manby, and M. Schütz, WIREs Comput. Mol. Sci. **2**, 242 (2012).
[29] F. H. Stillinger and T. A. Weber, Phys. Rev. B **31**, 5262 (1985).
[30] T. Watanabe, H. Fujiwara, H. Noguchi, T. Hoshino, and I. Ohdomari, Jpn. J. Appl. Phys., Part 2 **38**, L366 (1999).
[31] L. D. Landau and E. M. Lifshitz, *Mechanics*, 3rd ed. (Butterworth-Heinemann, Oxford, 1976), p. 170.
[32] H. Goldstein, *Classical Mechanics*, 3rd ed. (Addison-Wesley, Reading, MA, 1950), p. 672.
[33] G. G. Balint-Kurti and A. P. Palov, *Theory of Molecular Collision* (Royal Society of Chemistry, Cambridge, 2015), p. 282.
[34] W. Eckstein, S. Hackel, D. Heinemann, and B. Fricke, Z. Phys. D **24**, 171 (1992).
[35] M. T. Robinson, Radiat. Eff. Defects Solids **141**, 1 (1997).
[36] W. Eckstein and H. M. Urbassek, *Topics in Applied Physics*, edited by R. Behrisch and W. Eckstein (Springer, Berlin, 2007), Vol. 110, pp. 21–32.
[37] N. F. Mott and H. S. W. Massey, *The Theory of Atomic Collisions* (Clarendon, Oxford, 1965), p. 858.
[38] R. E. Langer, Phys. Rev. **51**, 0669 (1937).
[39] V. V. Pletnev, Vacuum **44**, 935 (1993).
[40] J. W. Coburn, H. F. Winters, and T. J. Chuang, J. Appl. Phys. **48**, 3532 (1977).
[41] P. Varga, T. Neidhart, M. Sporn, G. Libiseller, M. Schmid, F. Aumayr, and H. P. Winter, Phys. Scr. **1997**, 307 (1997).
[42] S. A. Norris, J. Samela, L. Bukonte, M. Backman, F. Djurabekova, K. Nordlund, C. S. Madi, M. P. Brenner, and M. J. Aziz, Nat. Commun. **2**, 276 (2011).